

Supporting Information

Contents

Experimental Section	
Fig. S1. ¹ H NMR spectrum of L ¹ in CDCl ₃ at 25 °C	2
Fig. S2. ¹³ C NMR spectrum of L ¹ in CDCl ₃ at 25 °C.	2
Fig. S3. FT-IR spectrum of L ¹ (KBr method) at 25 °C	3
Fig. S4. ¹ H NMR spectrum of L ² in CDCl ₃ at 25 °C.	3
Fig. S5. ¹³ C NMR spectrum of L ² in CDCl ₃ at 25 °C at 25 °C.	4
Fig. S6. FT-IR spectrum of L ² (KBr method) at 25 °C	4
Fig. S7. ¹ H NMR spectrum of L ³ in CDCl ₃ at 25 °C.	5
Fig. S8. ¹³ C NMR spectrum of L ³ in CDCl ₃ at 25 °C at 25 °C	5
Fig. S9. FT-IR spectrum of L ³ (KBr method) at 25 °C	6
Fig. S10. ¹ H NMR spectrum of 1 in DMSO- <i>d</i> ₆ at 25 °C.	6
Fig. S11. FT-IR spectrum of 1 at 25 °C (KBr method).	7
Fig. S12. ¹ H NMR spectrum of 2 in DMSO- <i>d</i> ₆ at 25 °C.	7
Fig. S13. FT-IR spectrum of 2 at 25 °C (KBr method).	8
Fig. S14. ¹ H NMR spectrum of 3 in DMSO- <i>d</i> ₆ at 25 °C	8
Fig. S15. FT-IR spectrum of 3 (KBr method) at 25 °C.	9
Fig. S16. ¹ H NMR spectrum of 4 in DMSO- <i>d</i> ₆ at 25 °C	9
Fig. S17. FT-IR spectrum of 4 at 25 °C (KBr method).	10
Fig. S18. ¹ H NMR spectrum of 5 in DMSO- <i>d</i> ₆ at 25 °C	10
Fig. S19. FT-IR spectrum of 5 at 25 °C (KBr method).	11
Fig. S20. ¹ H NMR spectrum of 6 in DMSO- <i>d</i> ₆ at 25 °C	11
Fig. S21. FT-IR spectrum of 6 at 25 °C (KBr method).	12
Fig. S22. ¹ H NMR spectrum of 7 in DMSO- <i>d</i> ₆ at 25 °C.	12
Fig. S23. FT-IR spectrum of 7 at 25 °C (KBr method)	13
Fig. S24. ¹ H NMR spectrum of 1a in CDCl ₃ at 25 °C	13
Fig. S25. ¹ H NMR spectrum of 1b in CDCl ₃ at 25 °C.	14
Fig. S26. ¹ H NMR spectrum of 1c in CDCl ₃ at 25 °C.	14
Fig. S27. ¹ H NMR spectrum of 1d in DMSO- <i>d</i> ₆ at 25 °C.	15
Fig. S28. ¹ H NMR of 1e in CDCl ₃ at 25 °C.	15
Fig. S29. ¹ H NMR of 1f in CDCl ₃ at 25 °C.	16
Fig. S30. ¹ H NMR of 1g in CDCl ₃ at 25 °C.	16
Fig. S31. ¹ H NMR of 1h in CDCl ₃ at 25 °C.	17
Fig. S32. Effect of catalyst 7 loading on [3+2] cycloaddition reaction between mesityl azide and phenylacetylene at ambient temperature, 2 h in DCM and MeOH mixture.	17
Fig. S33. FT-IR spectra of a mixture of phenylacetylene and mesityl azide in 0 min. and 120 min	18
Fig. S34. The thermal ellipsoidal structures of 1-7 . The hydrogen atoms have been omitted for clarity.	18-19
Table. S1 The structural parameter of 1-4	19-20
Table. S2 The structural parameter of 5-7	20
Table. S3 Selected bond lengths of 1-6	21
Table. S4 Selected bond angles of 1-6	21
Table. S5 Selected bond lengths and angles of 7	21
Table. S6. Comparison of catalytic efficiency of 7 with known Cu(I) catalysts for the formation of triazole product.	21-23

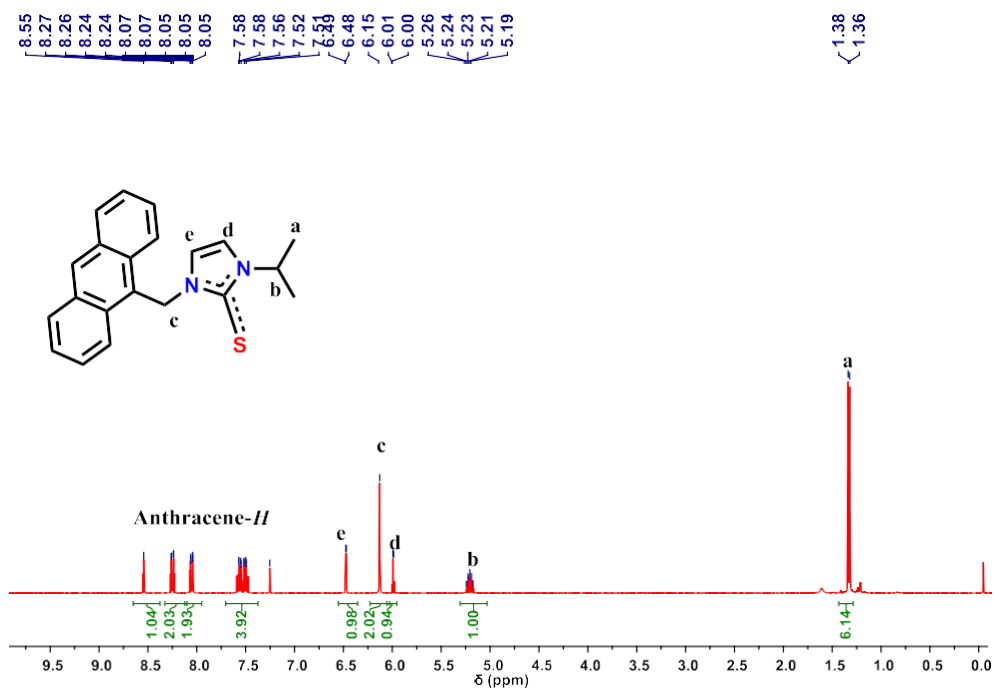


Fig. S1. ¹H NMR of L¹ in CDCl₃ at 25 °C

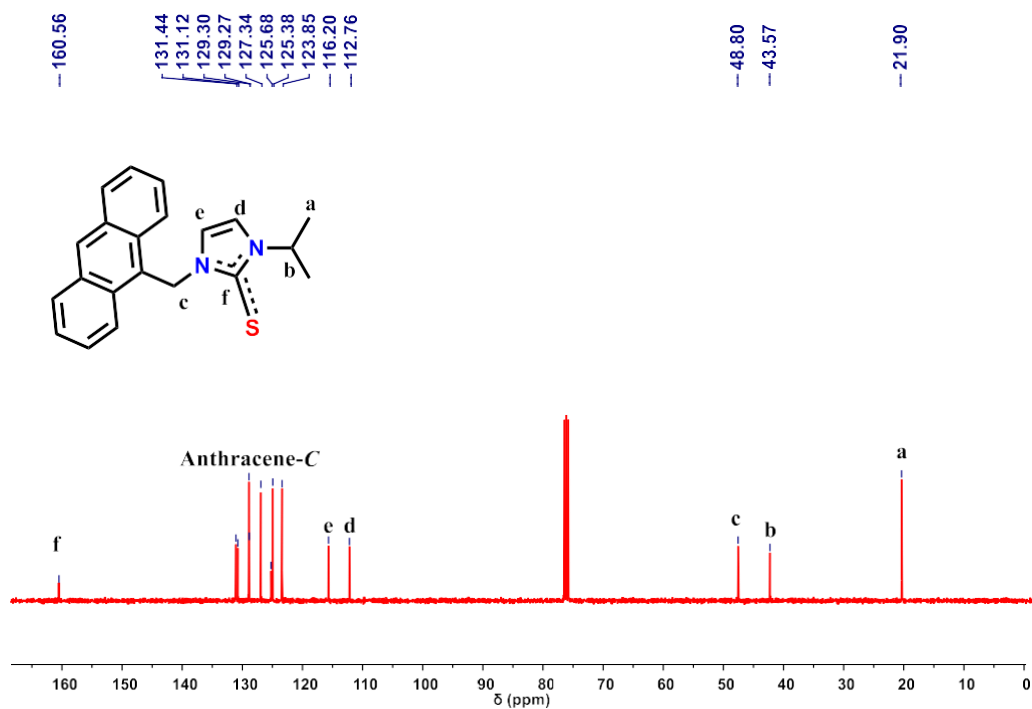


Fig. S2. ¹³C NMR of L¹ in CDCl₃ at 25 °C

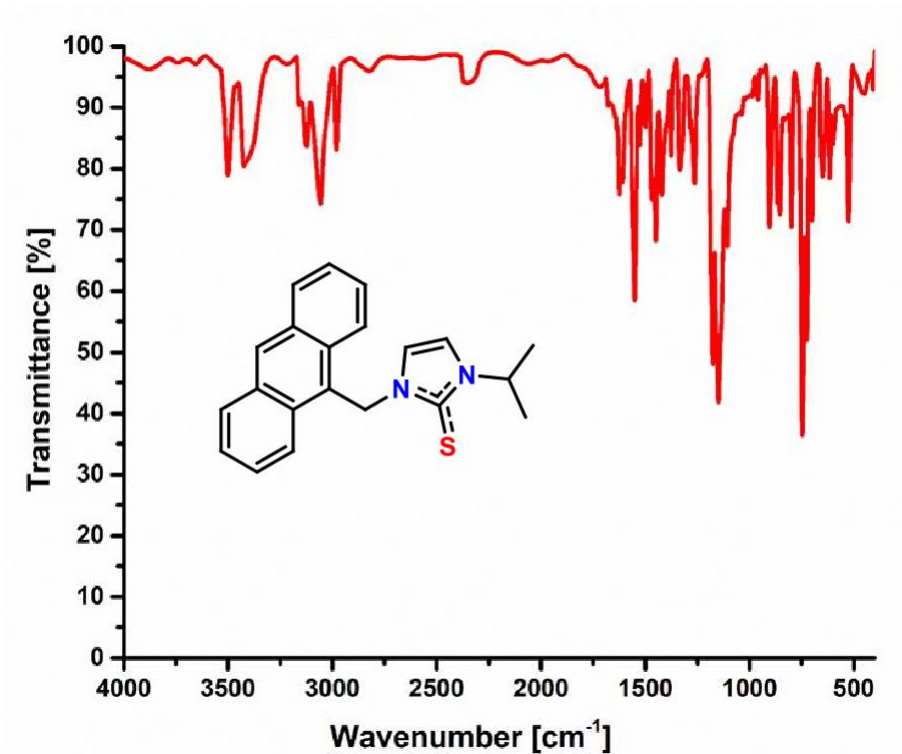


Fig. S3. FT-IR spectrum of L¹ (KBr method) at 25 °C

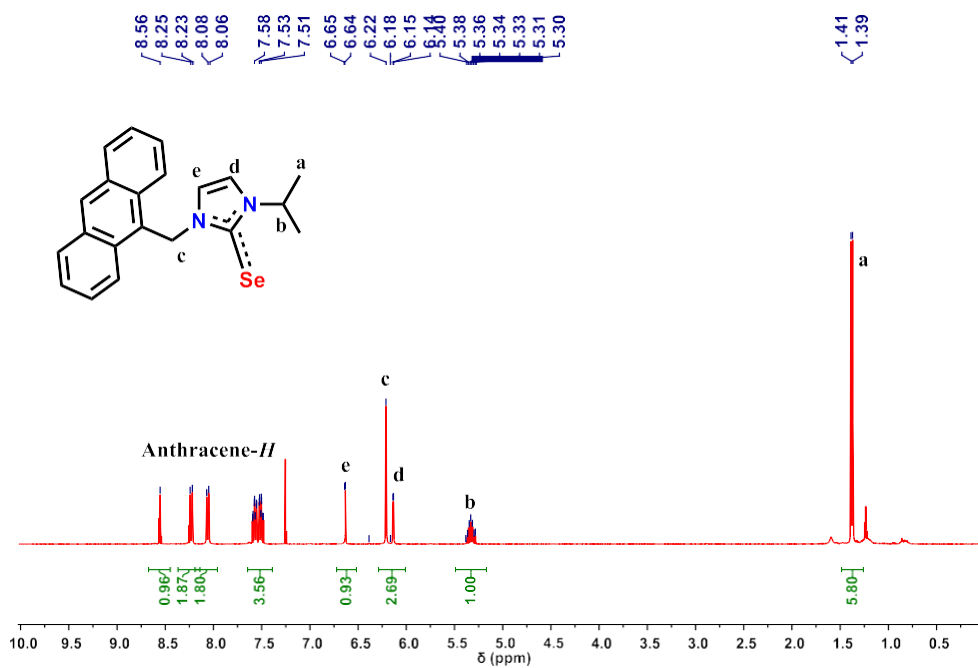


Fig. S4. ¹H NMR of L² in CDCl₃ at 25 °C

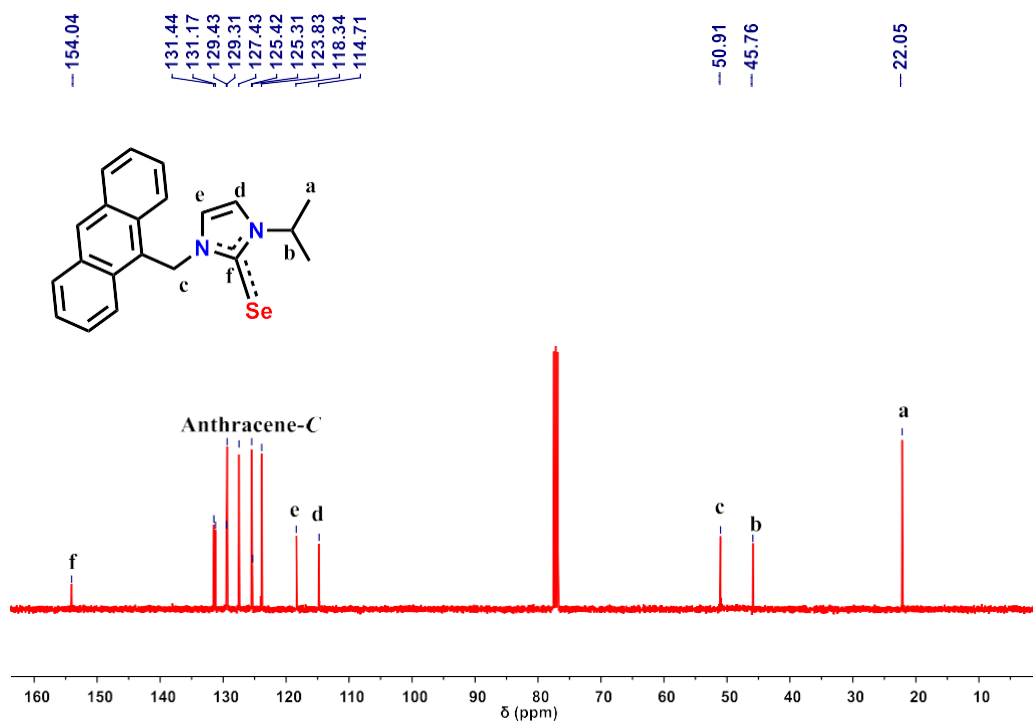


Fig. S5. ^{13}C NMR of L^2 in CDCl_3 at 25°C

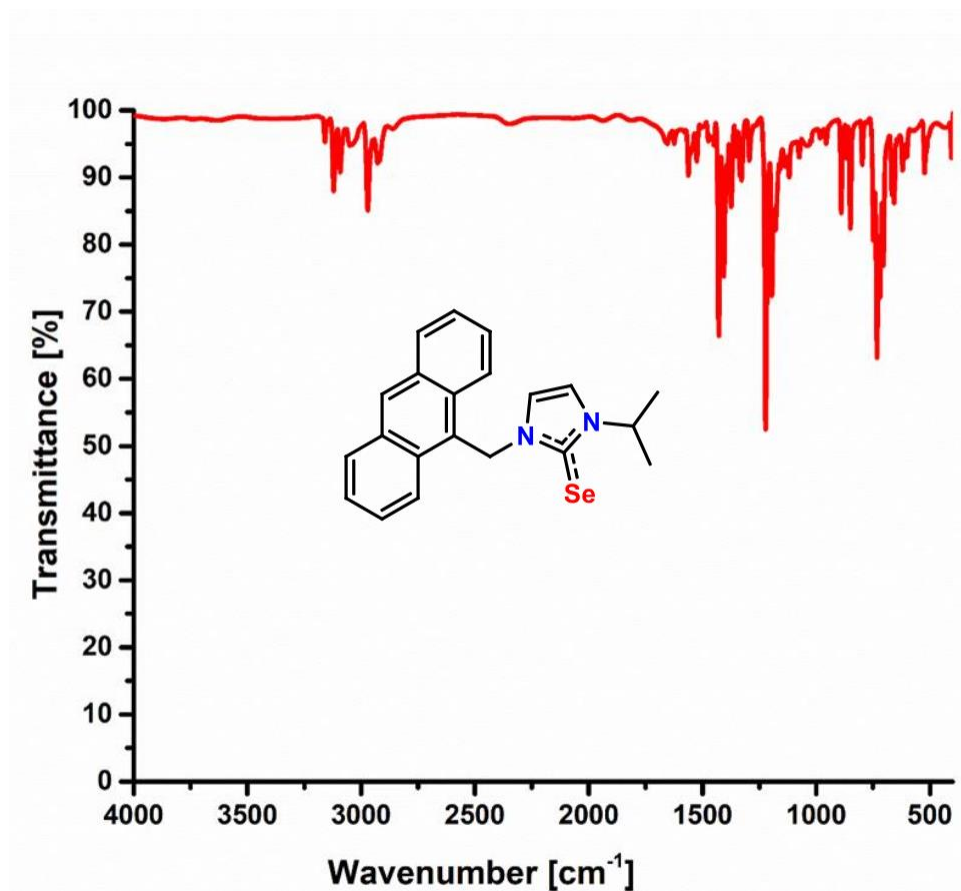


Fig. S6. FT-IR of L^2 (KBr method) at 25°C

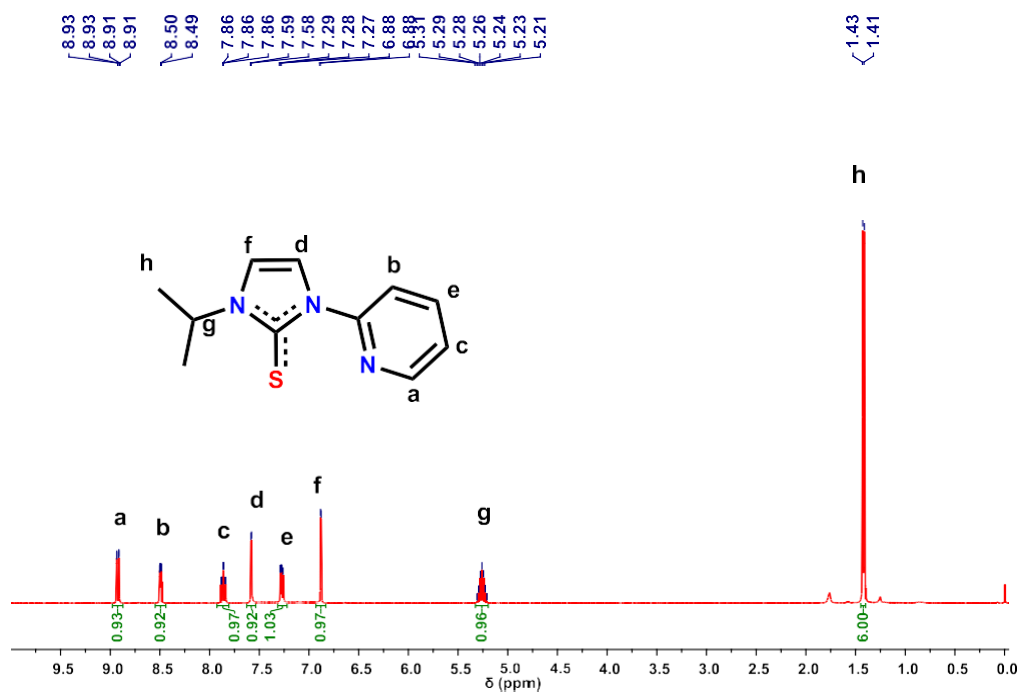


Fig. S7. ^1H NMR of L^3 in CDCl_3 at 25°C

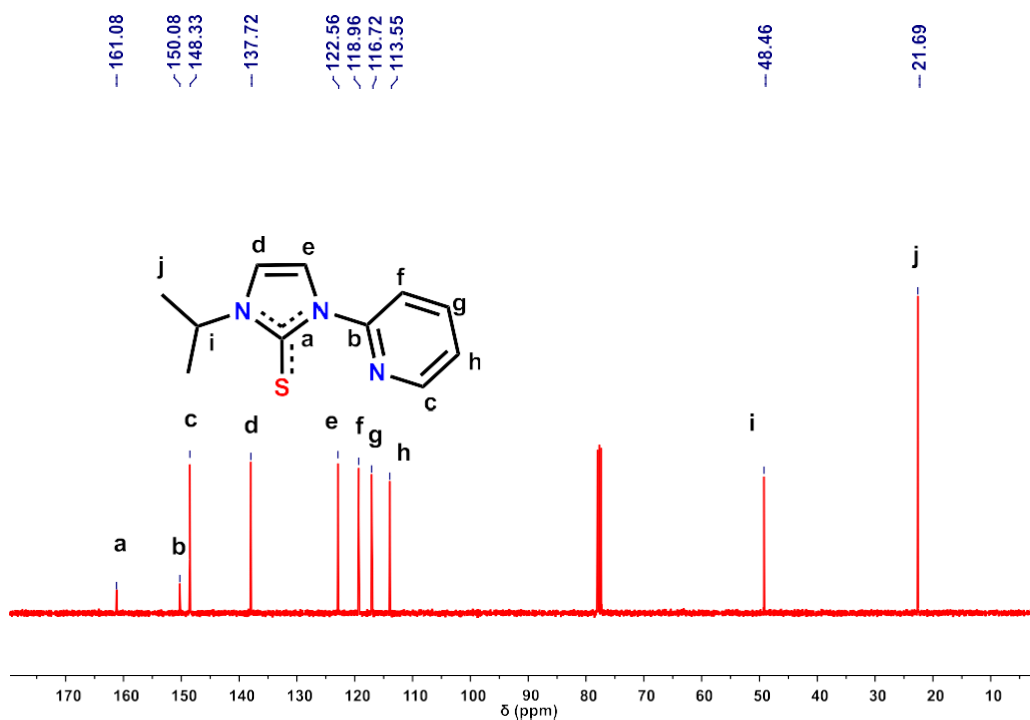


Fig. S8. ^{13}C NMR of L^3 in CDCl_3 at 25°C

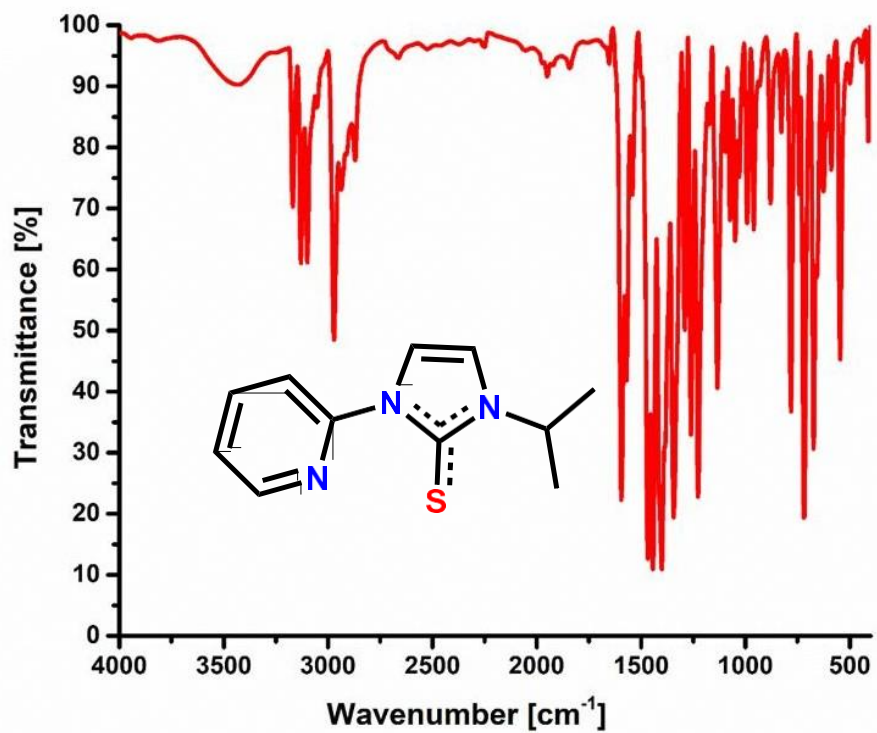


Fig. S9. FT-IR spectrum of L^3 (KBr method) at 25 °C

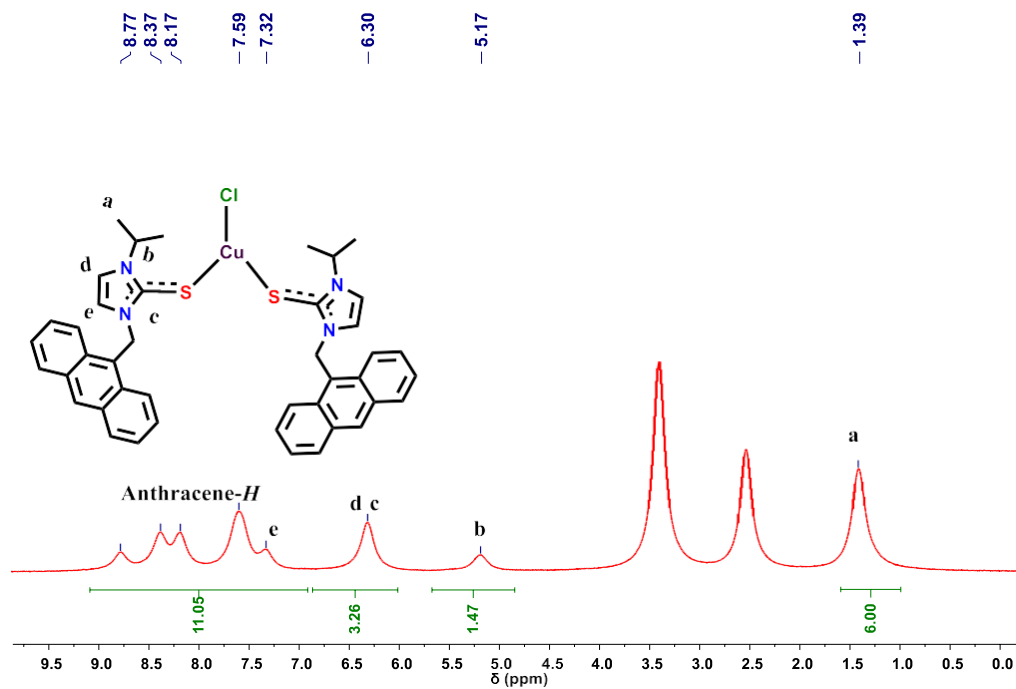


Fig. S10. ^1H NMR of **1** in $\text{DMSO-}d_6$ at 25 °C

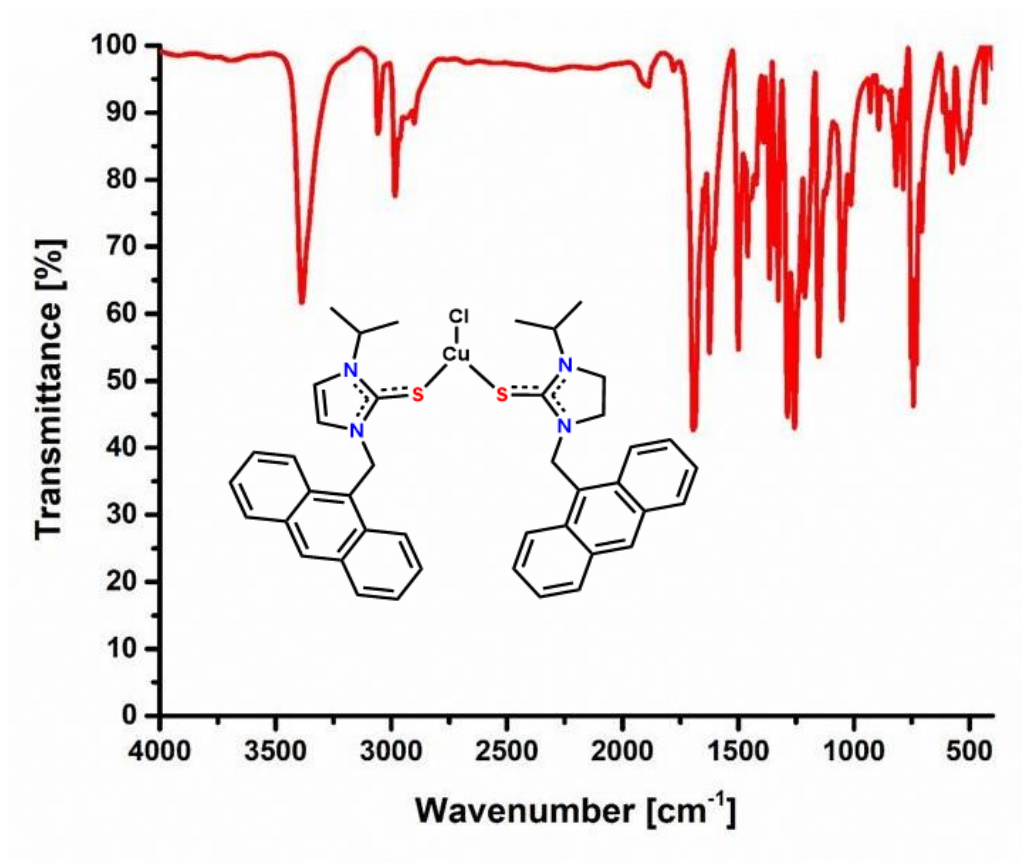


Fig. S11. FT-IR spectrum of **1** (KBr method) at 25 °C

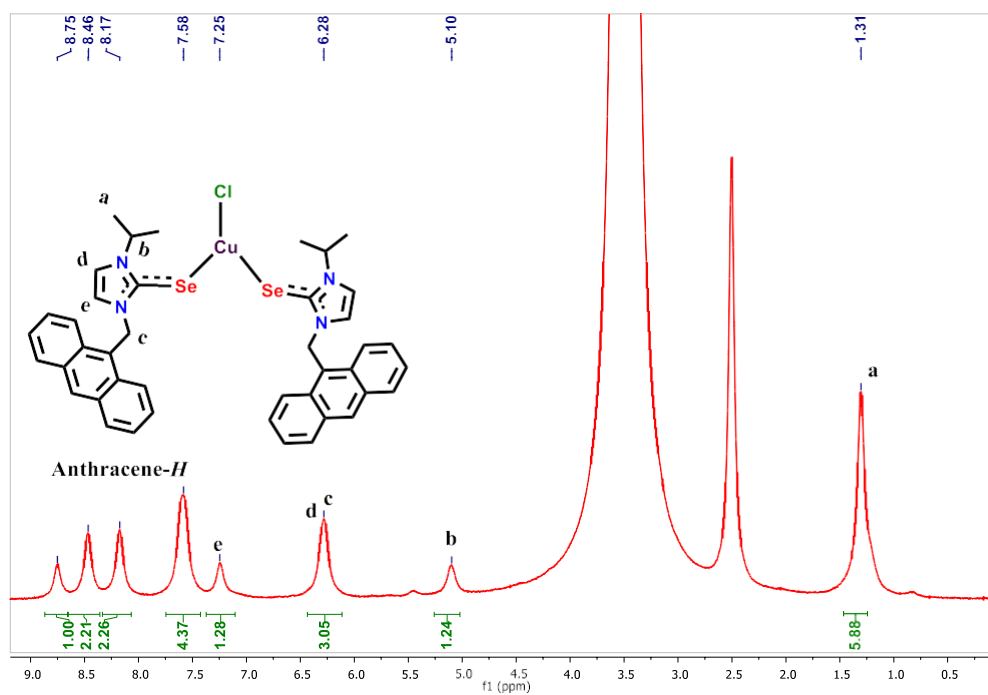


Fig S12. ^1H NMR of **2** in $\text{DMSO}-d_6$ at 25 °C

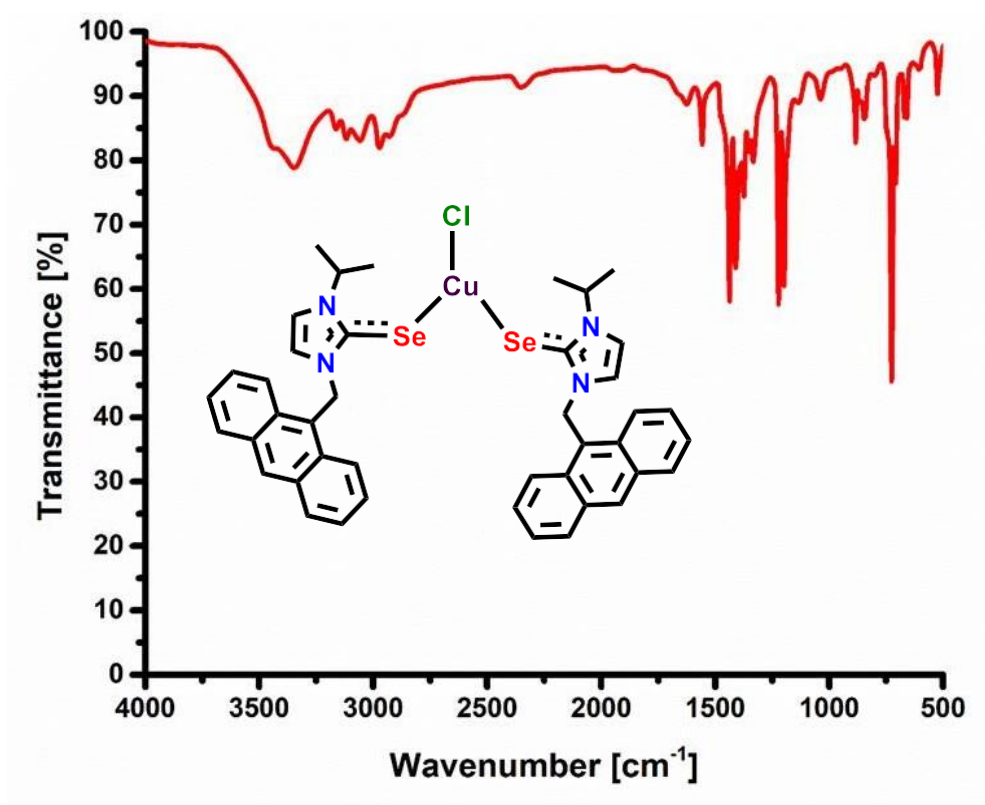


Fig. S13. FT-IR spectrum of **2** (KBr method) at 25 °C

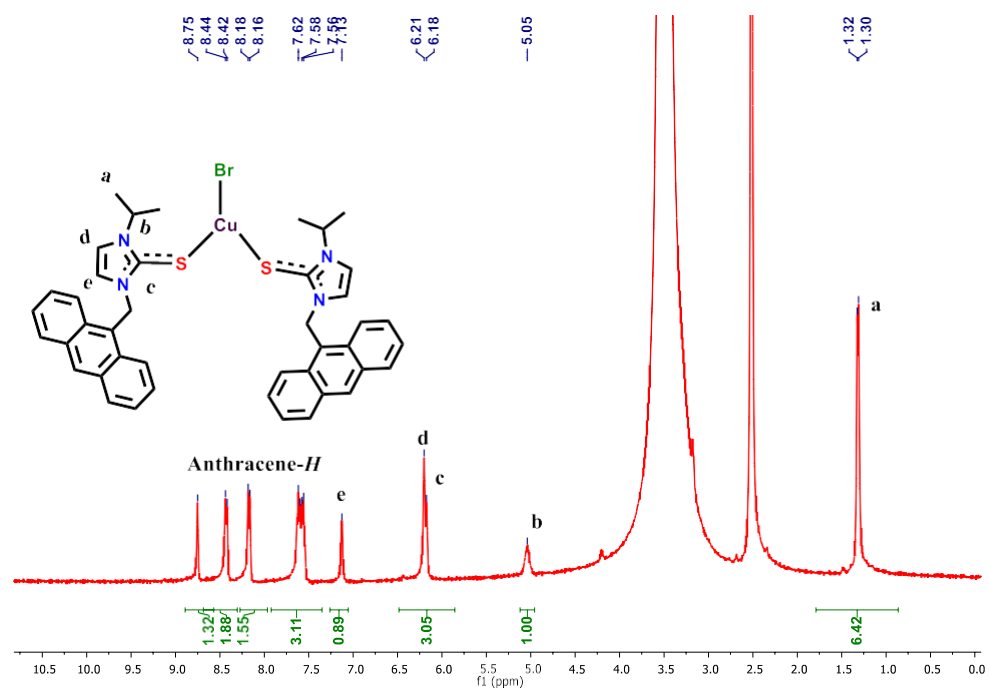


Fig. S14. ^1H NMR of **3** in $\text{DMSO-}d_6$ at 25 °C

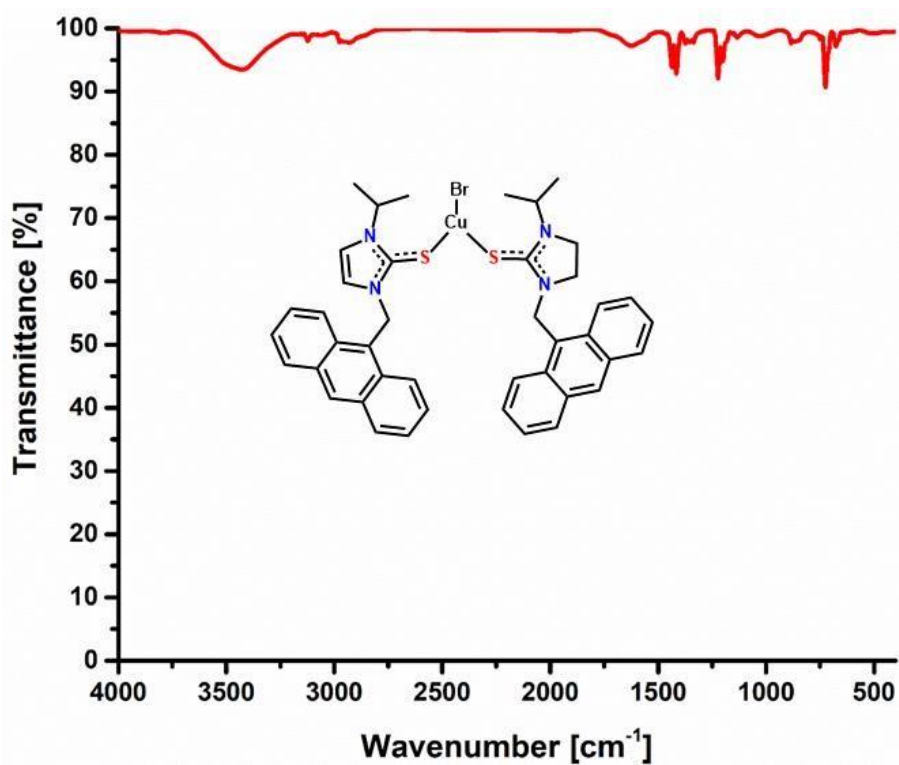


Fig. S15. FT-IR spectrum of **3** (KBr method) at 25 °C

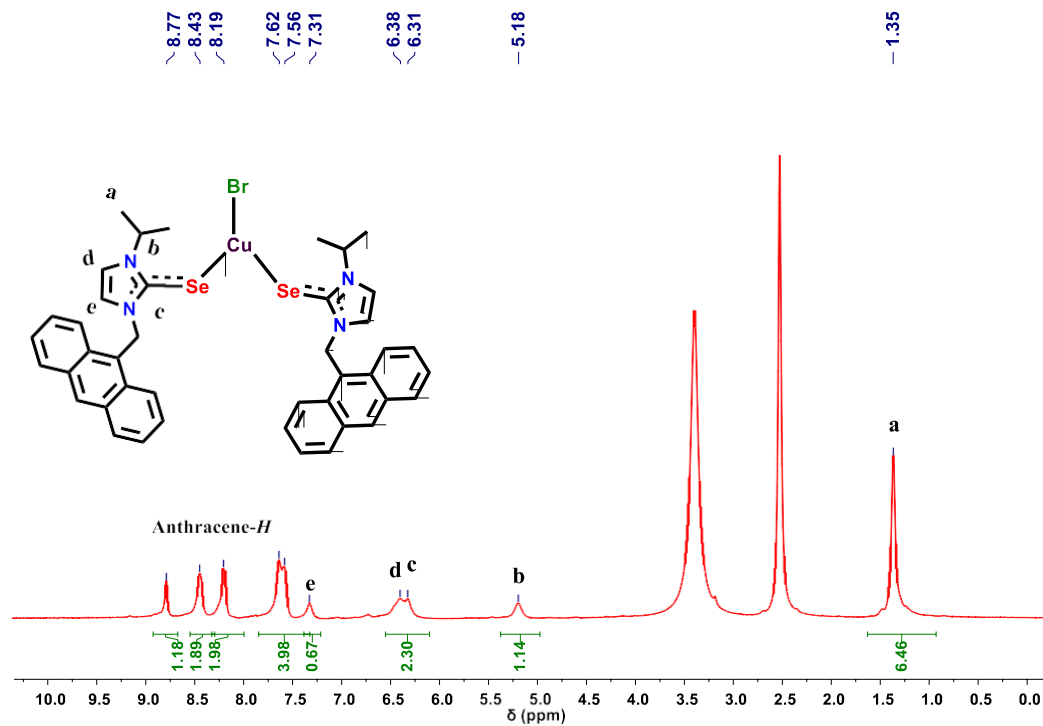


Fig. S16. ^1H NMR of **4** in $\text{DMSO-}d_6$ at 25 °C

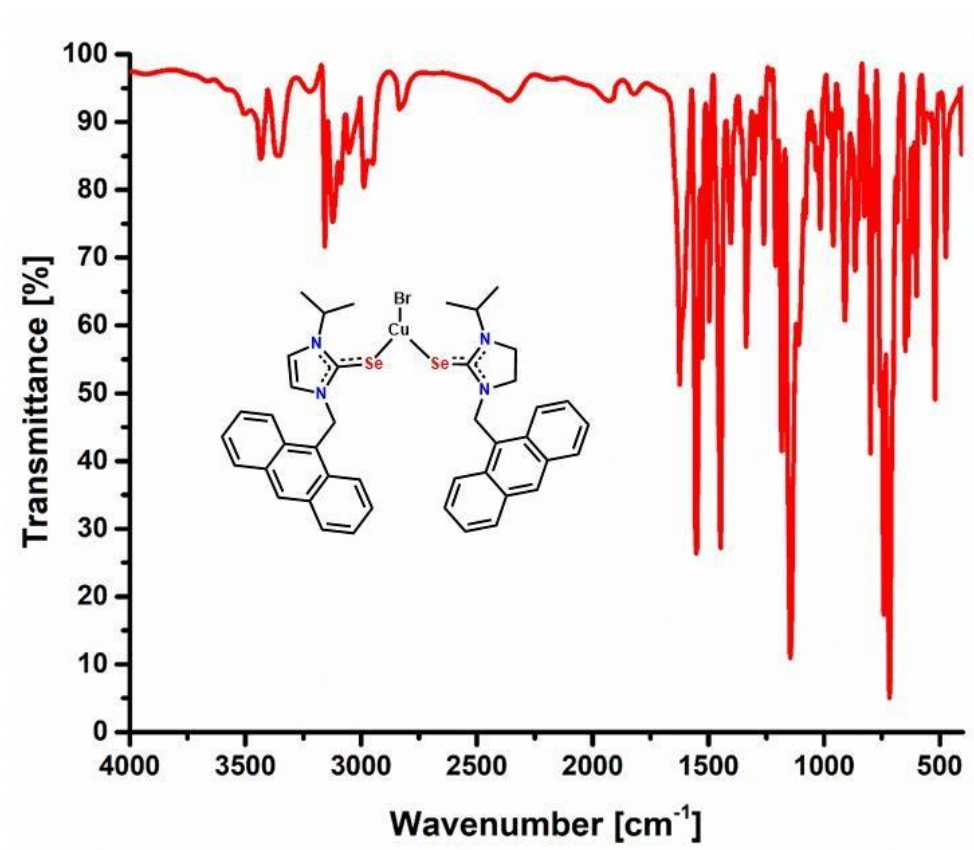


Fig. S17. FT-IR spectrum of **4** (KBr method) at 25 °C

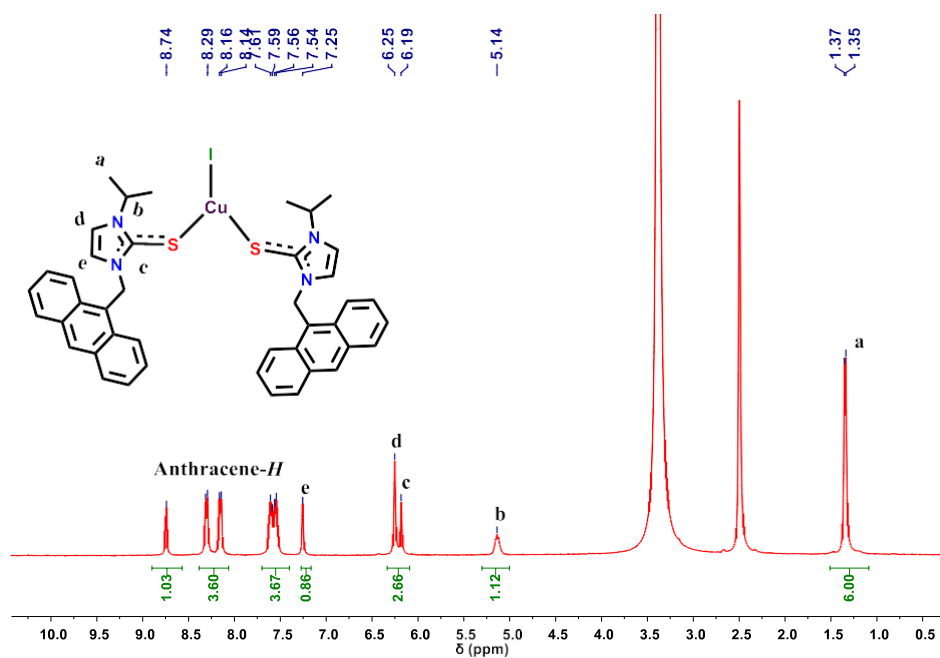


Fig. S18. ^1H NMR of **5** in $\text{DMSO-}d_6$ at 25 °C

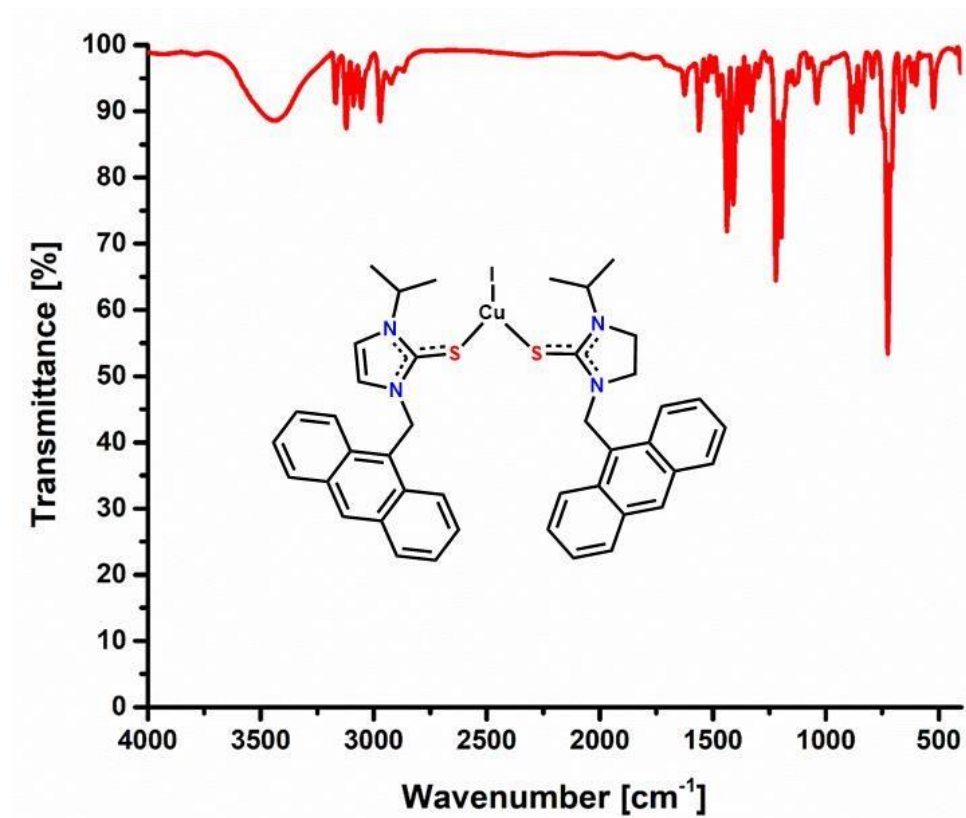


Fig. S19. FT-IR spectrum of 5 (KBr method) at 25 °C

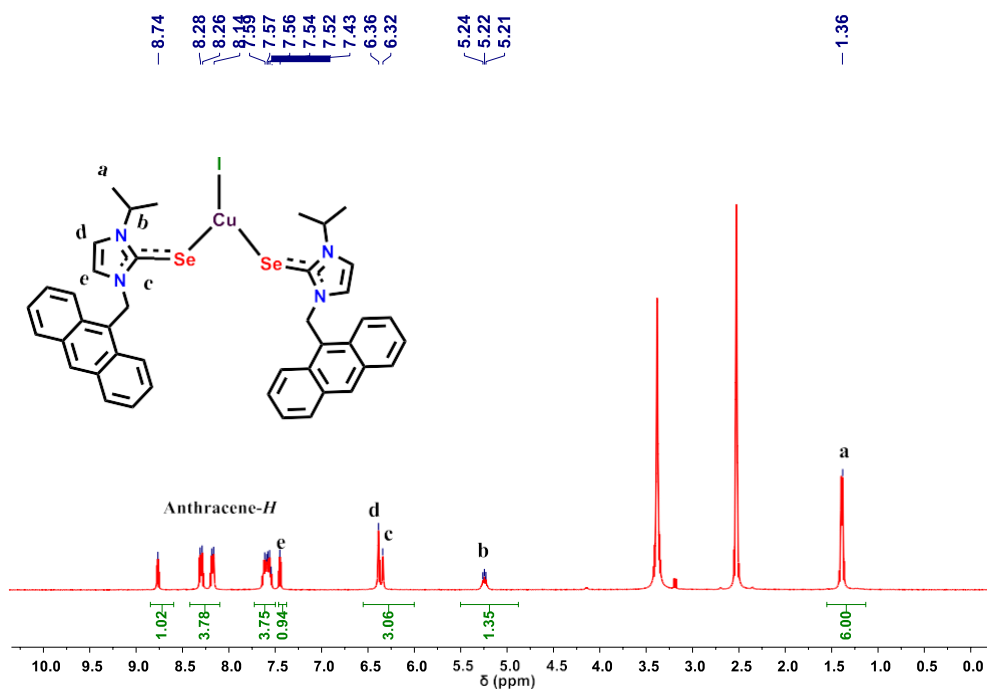


Fig S20. ^1H NMR of 6 in $\text{DMSO-}d_6$ at 25 °C

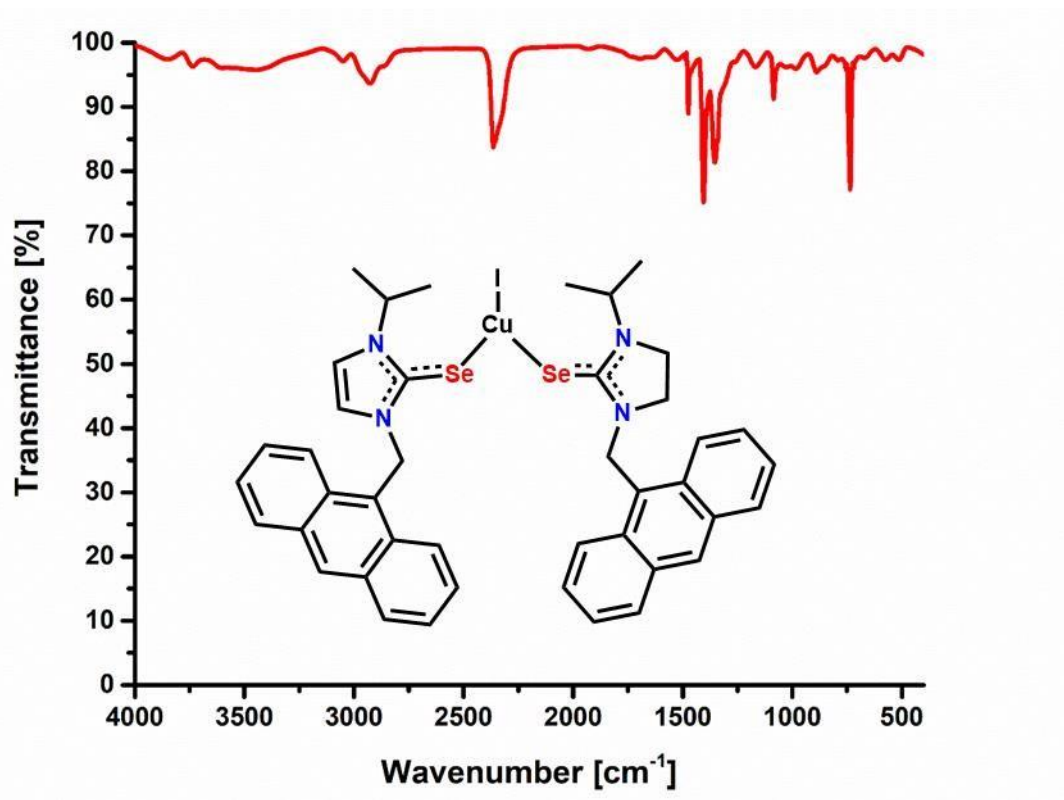


Fig. S21. FT-IR spectrum of **6** (KBr method) at 25 °C

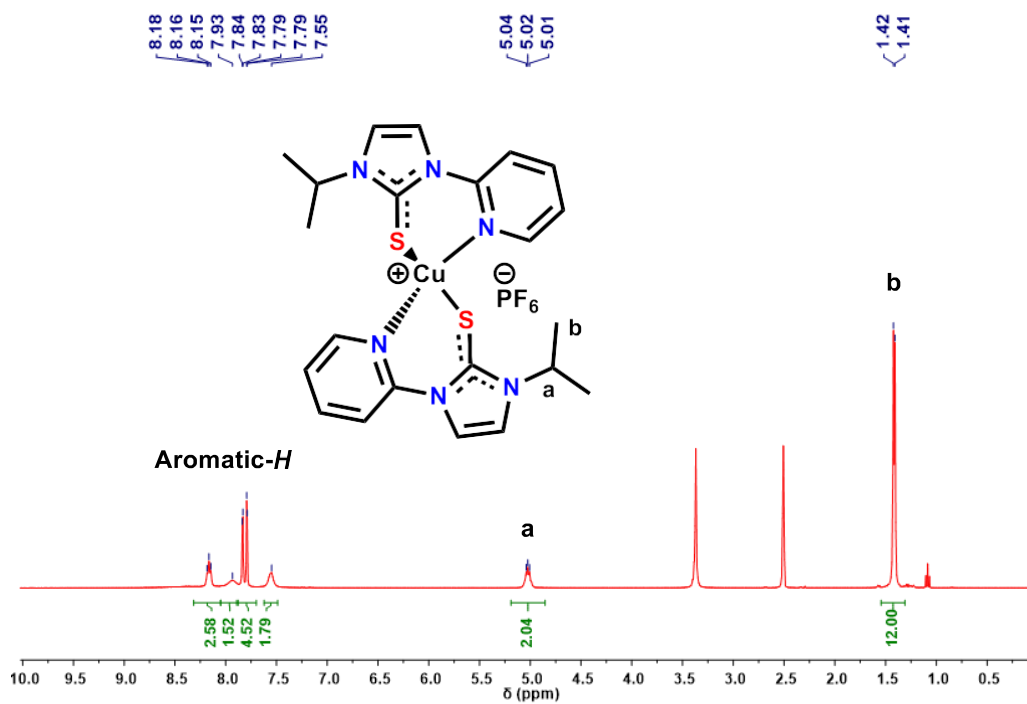


Fig. S22. ^1H NMR of **7** in $\text{DMSO-}d_6$ at 25 °C

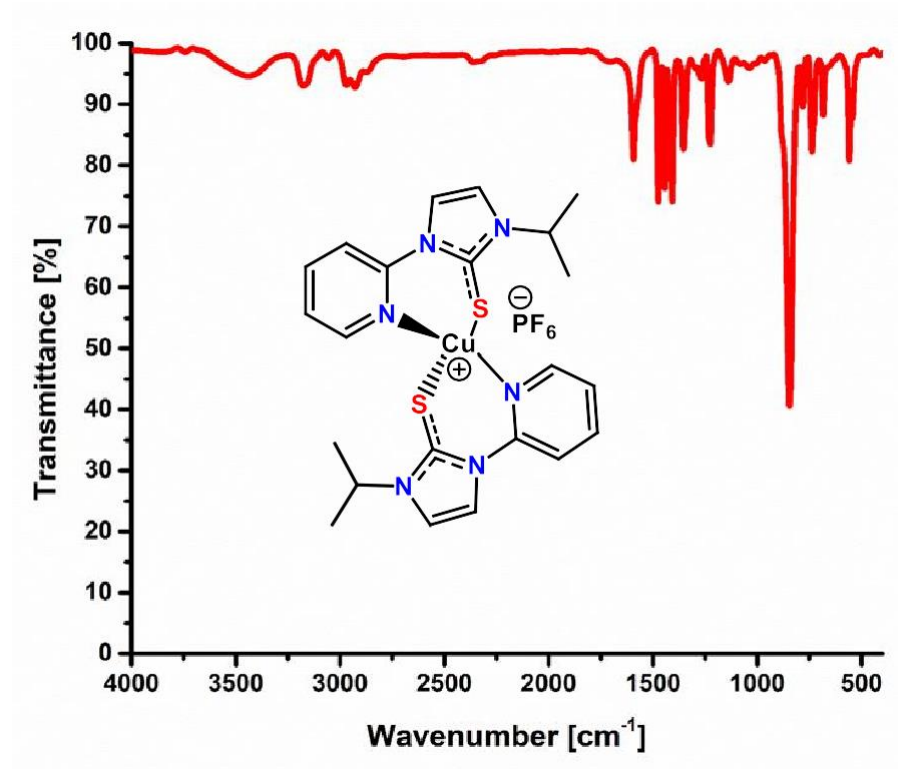


Fig. S23. FT-IR spectrum of 7 (KBr method) at 25 °C

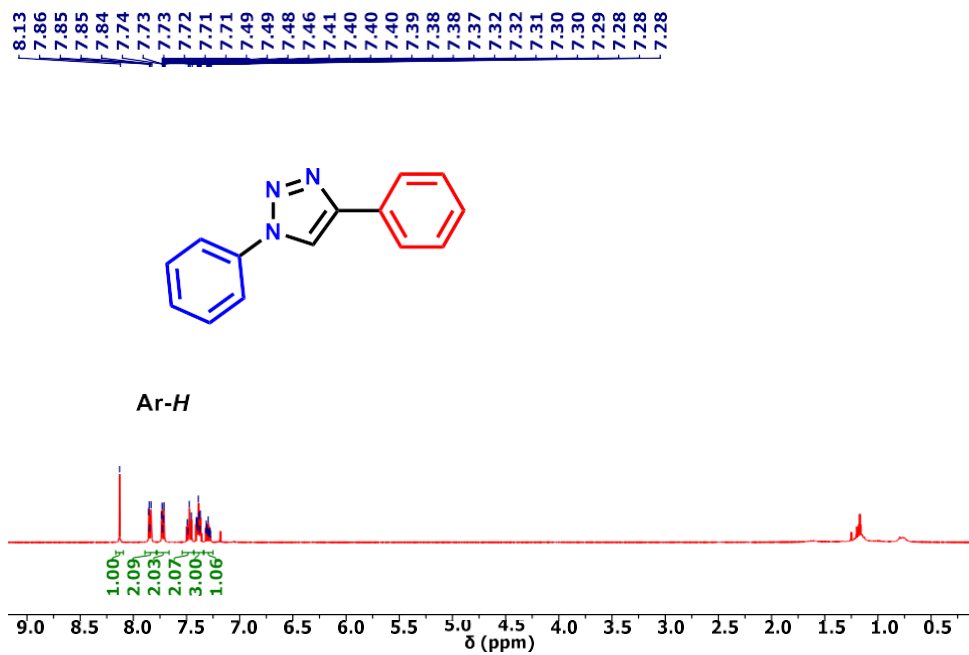


Fig. S24. ^1H NMR of 1a in CDCl_3 at 25 °C

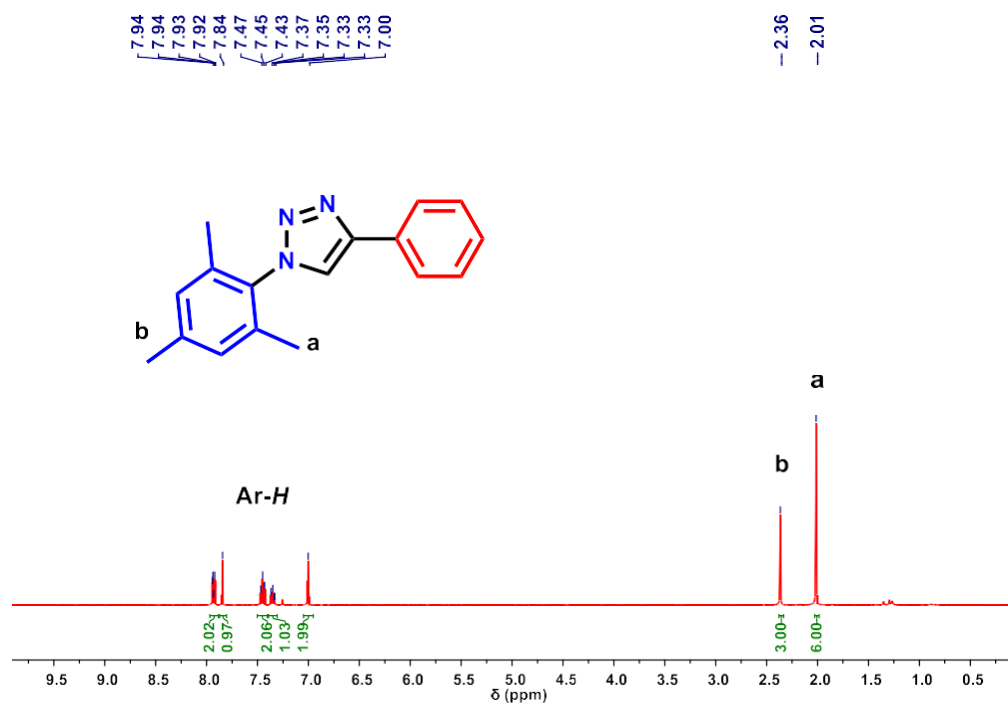


Fig. S25. ¹H NMR of **1b** in CDCl₃ at 25 °C.

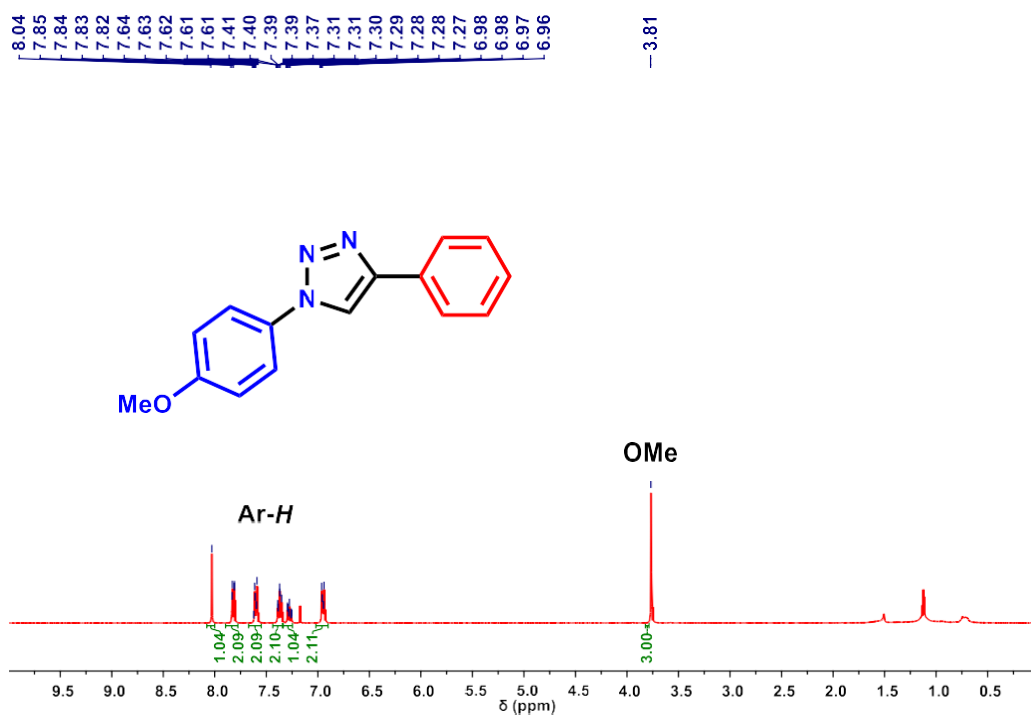


Fig. S26. ¹H NMR of **1c** in CDCl₃ at 25 °C.

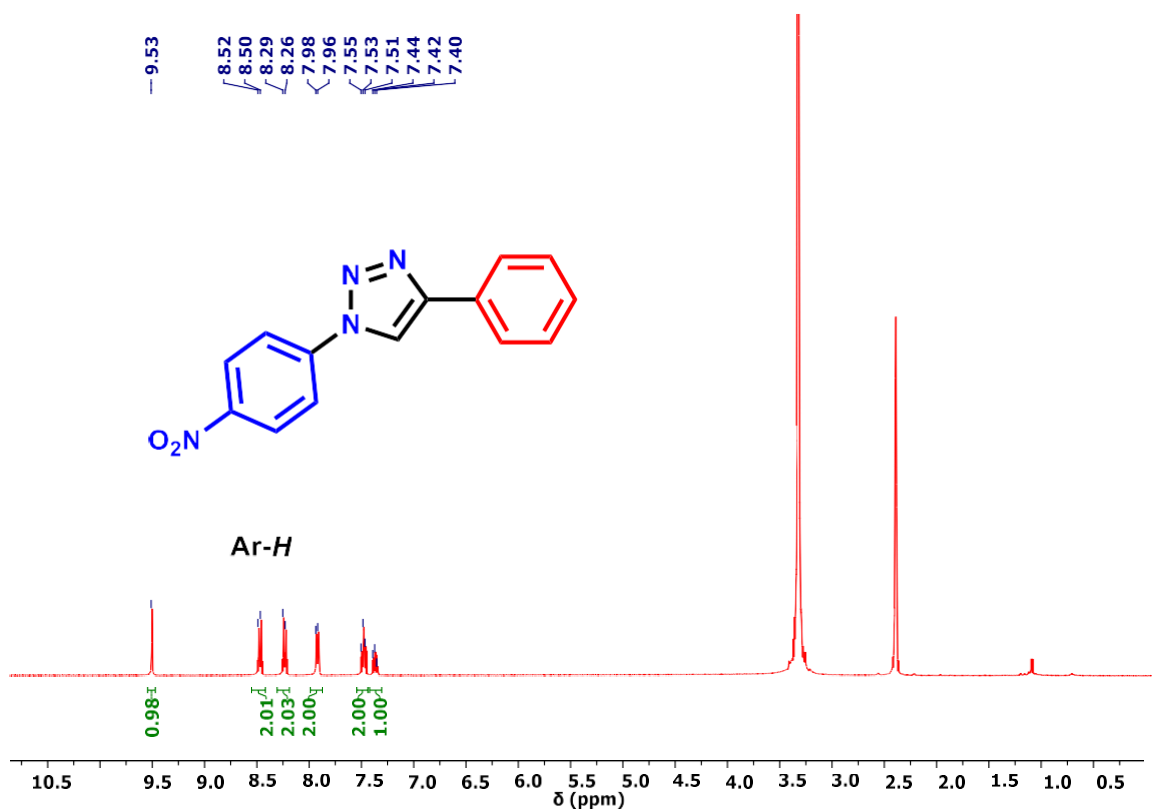


Fig. S27. $^1\text{H NMR}$ of 1d in $\text{DMSO-}d_6$ at $25\text{ }^\circ\text{C}$

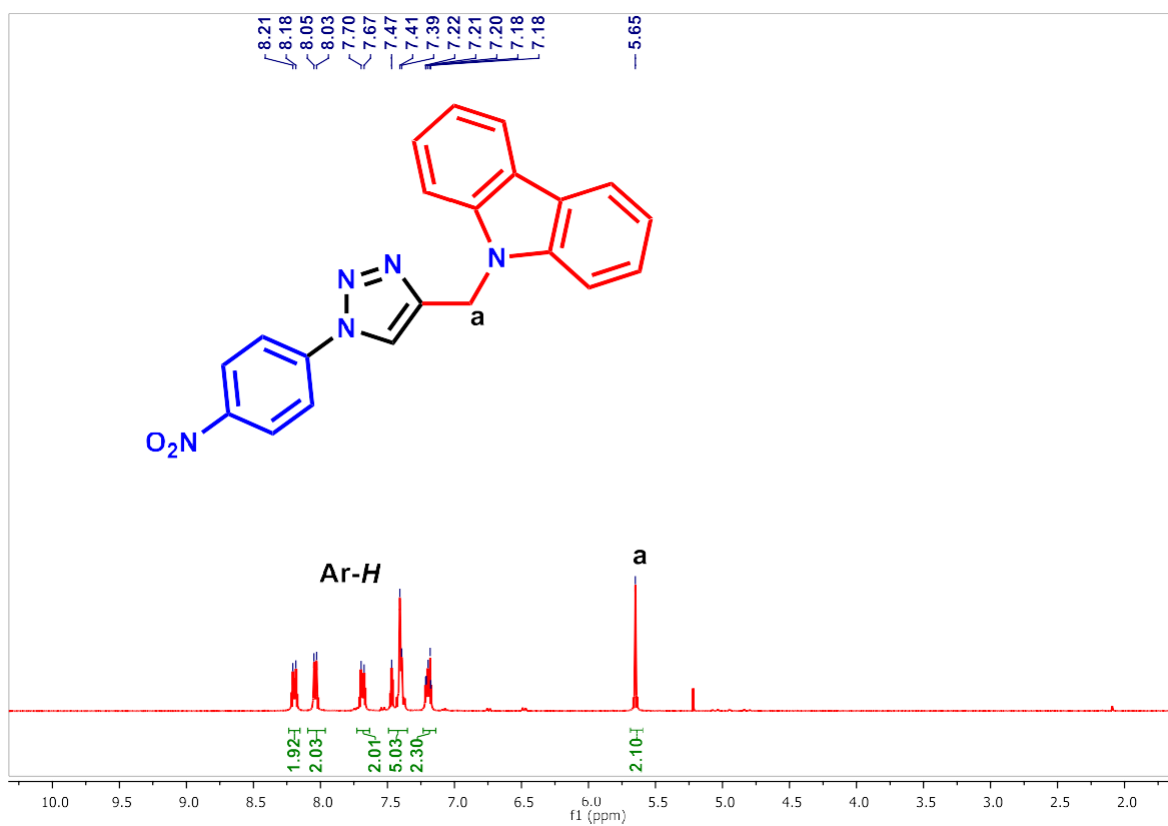


Fig. S28. $^1\text{H NMR}$ of 1e in CDCl_3 at $25\text{ }^\circ\text{C}$.

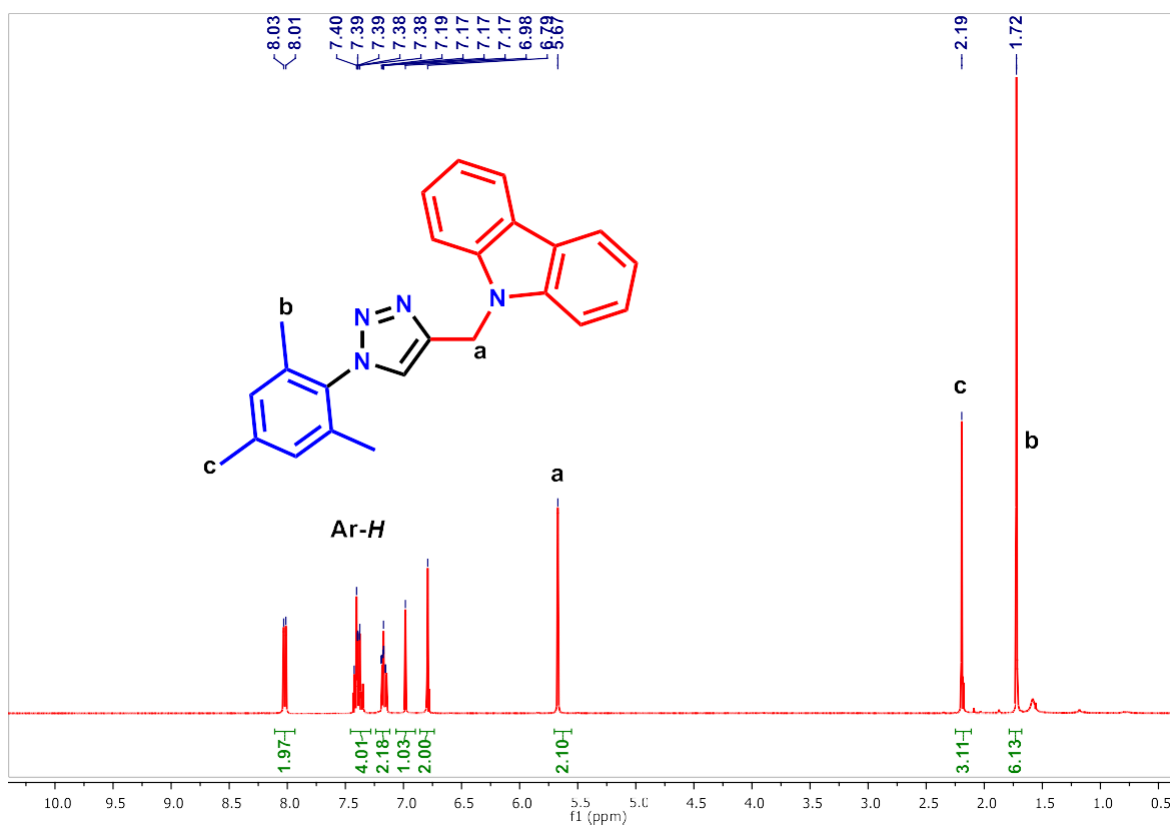


Fig. S29. ^1H NMR of **1f** in CDCl_3 at 25 °C.

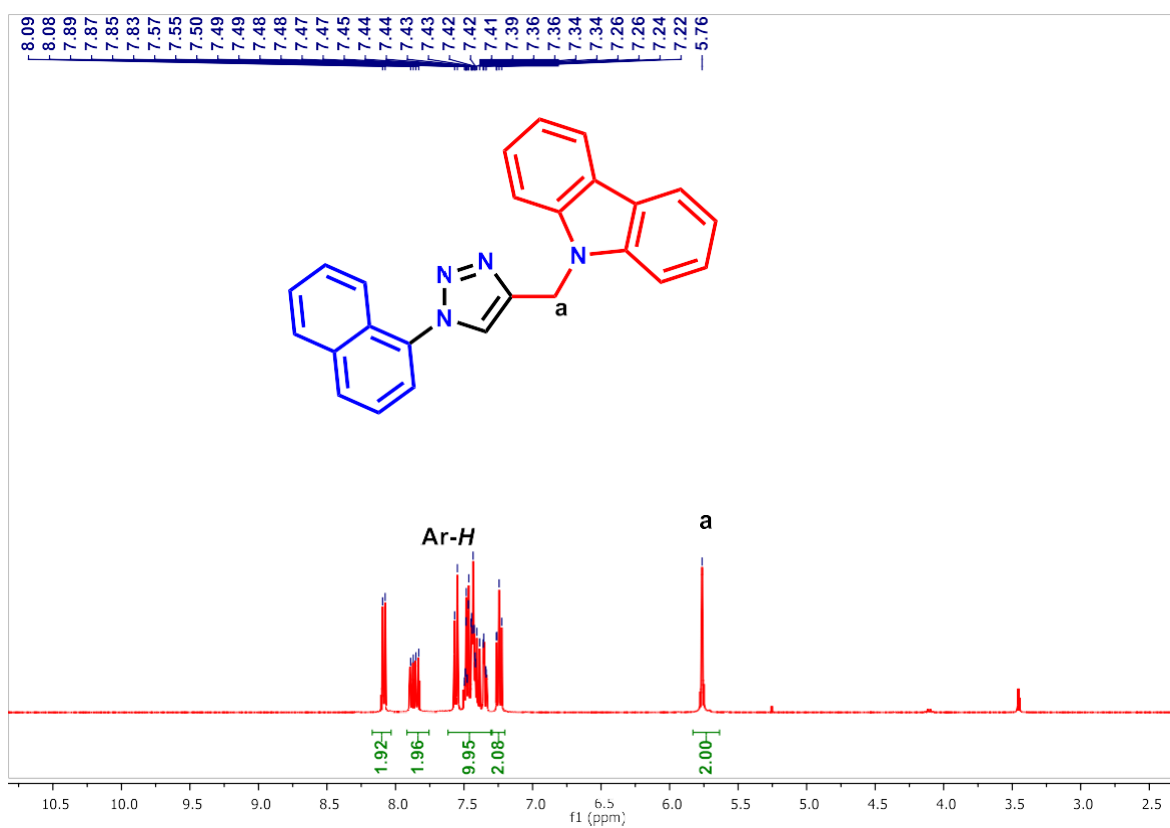


Fig. S30. ^1H NMR of **1g** in CDCl_3 at 25 °C.

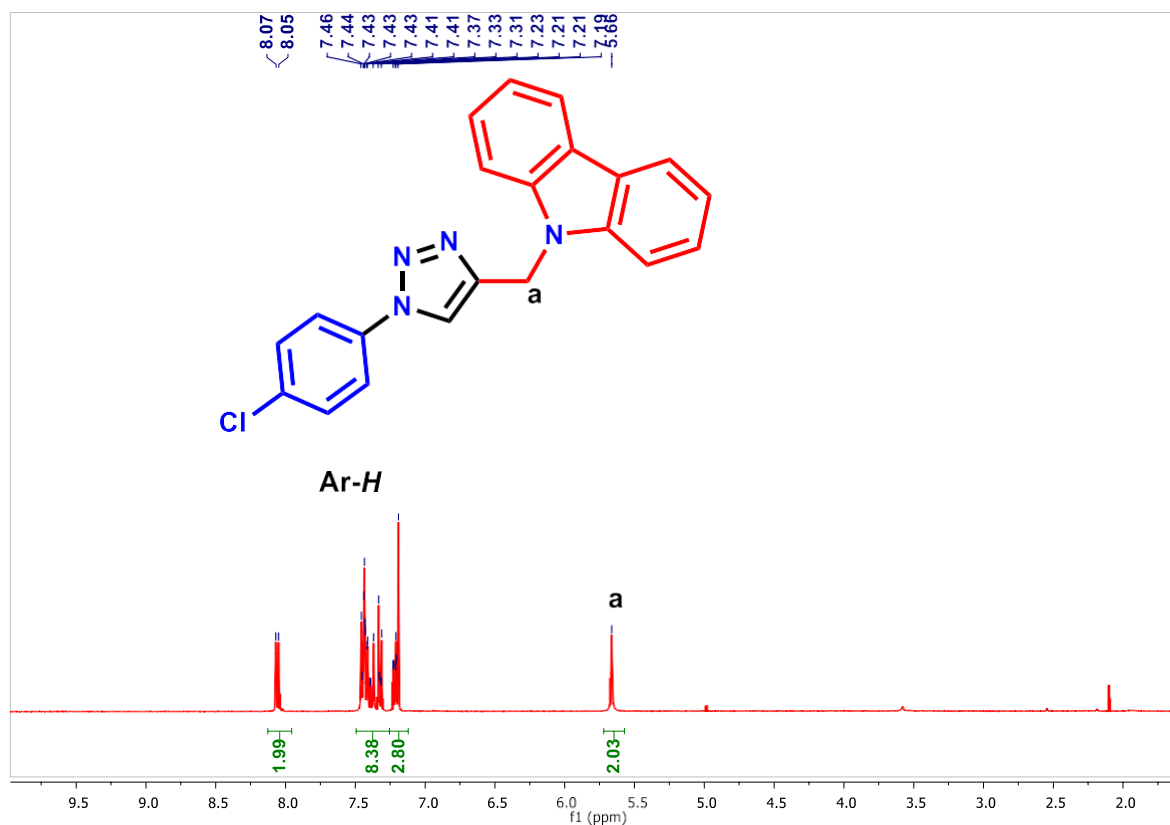


Fig. S31. $^1\text{H NMR}$ of **1h** in CDCl_3 at 25 °C

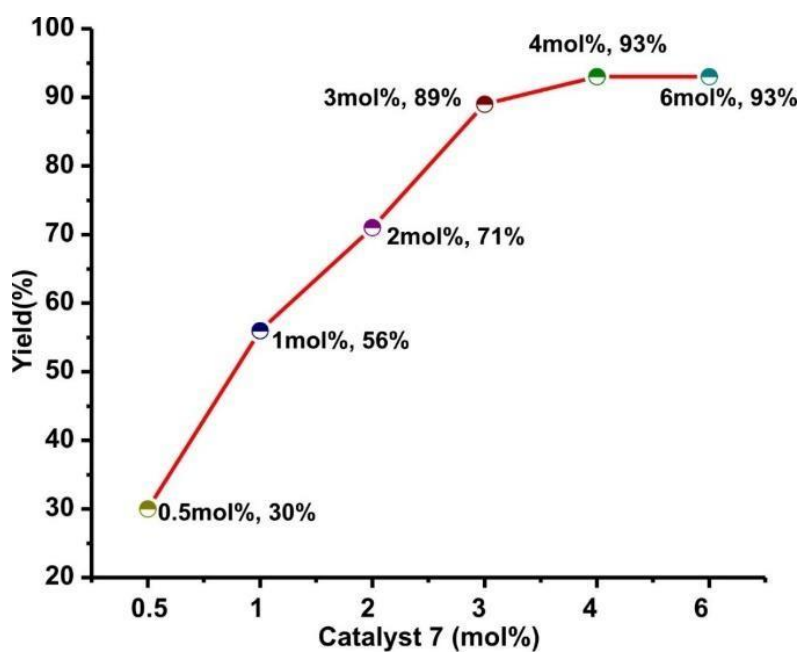


Fig. S32. Effect of catalyst **7** loading on [3+2] cycloaddition reaction between mesityl azide and phenylacetylene at ambient temperature, 2 h in DCM and MeOH mixture.

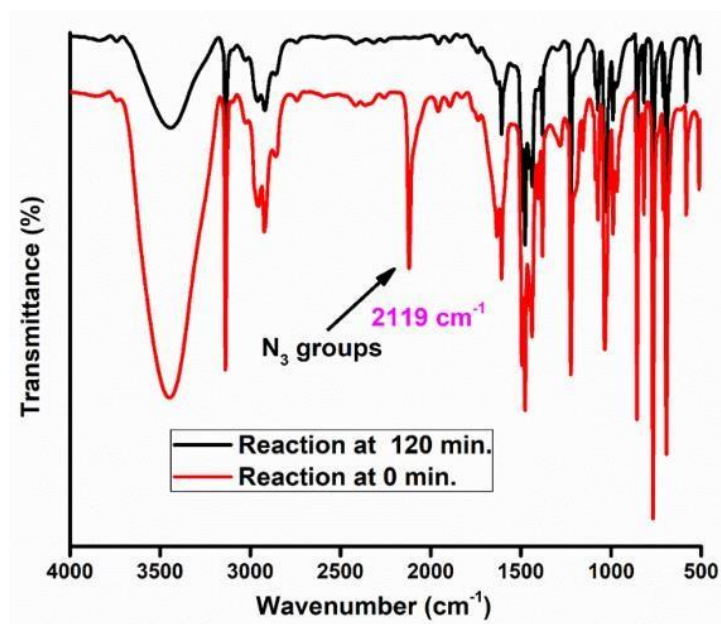
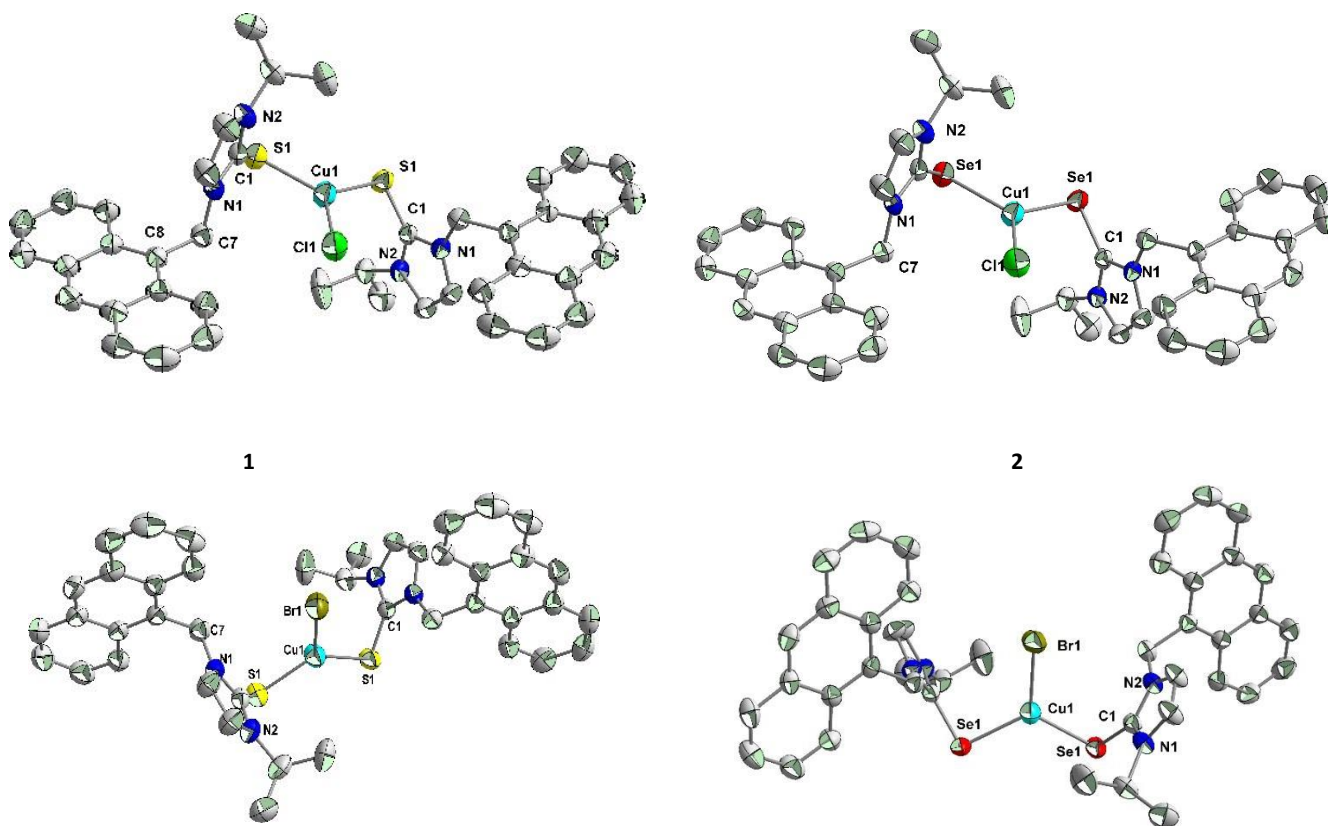


Fig. S33. FT-IR spectra of a mixture of phenylacetylene and mesityl azide in 0 min. and 120 min



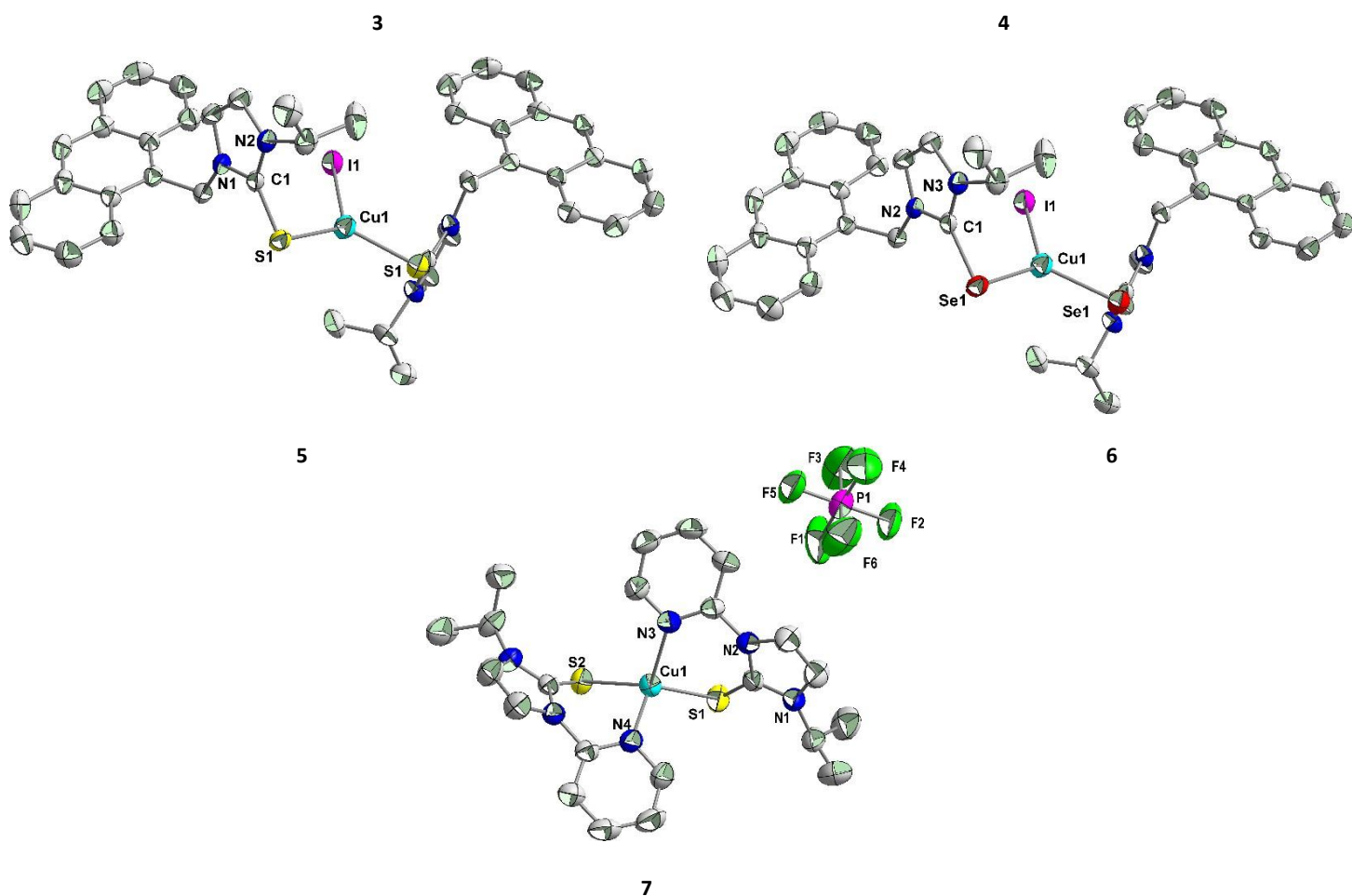


Fig. 34. The thermal ellipsoidal structures of 1-7. The hydrogen atoms have been omitted for clarity.

Table S1. The structural parameters of 1-4.

	1	2	3	4
Empirical formula	C ₄₂ H ₄₀ N ₄ S ₂ ClCu	C ₄₂ H ₄₀ N ₄ S ₂ ClCu	C ₄₂ H ₄₀ N ₄ S ₂ BrCu	C ₄₂ H ₄₀ N ₄ Se ₂ BrCu
Formula weight	763.89	857.69	812.35	902.15
Temperature/K	273.15	299	273.15	273.15
Crystal system	monoclinic	monoclinic	monoclinic	monoclinic
Space group	C2/c	C2/c	C2/c	C2/c
a/Å	28.019(3)	28.106(7)	28.070(16)	28.090(19)
b/Å	10.1880(9)	10.306(3)	10.219(5)	10.332(6)
c/Å	14.114(12)	14.197(3)	14.185(8)	14.202(9)
α/°	90	90	90	90
β/°	115.370(3)	116.160(10)	114.84(3)	115.758(4)
γ/°	90	90	90	90
Volume/Å ³	3640.4(6)	3691.6(16)	3693(3)	3712.5(4)
Z	4	4	4	4
ρ _{calc} /cm ³	1.394	1.543	1.461	1.614
μ/mm ⁻¹	0.825	2.672	1.825	3.662
F(000)	1592.0	1736.0	1672.0	1808.0
Crystal size/mm ³	0.117 × 0.065 × 0.035	0.28 × 0.25 × 0.17	0.28 × 0.17 × 0.17	0.28 × 0.17 × 0.17
Radiation	MoKα (λ=0.71073)	MoKα (λ=0.71073)	MoKα (λ = 0.71073)	MoKα (λ = 0.71073)

2 θ range for data collection/ $^{\circ}$	4.31 to 54.208	4.268 to 54.44	4.294 to 54.536	4.258 to 54.244
Index ranges	$-35 \leq h \leq 35, -13 \leq k \leq 13, -16 \leq l \leq 18$	$-35 \leq h \leq 36, -13 \leq k \leq 12, -18 \leq l \leq 16$	$-35 \leq h \leq 36, -10 \leq k \leq 13, -18 \leq l \leq 18$	$-36 \leq h \leq 36, -12 \leq k \leq 13, -18 \leq l \leq 18$
Reflections collected	29121	22075	31839	36317
Independent reflections	4013 [$R_{\text{int}} = 0.0945, R_{\text{sigma}} = 0.0580$]	4099 [$R_{\text{int}} = 0.0559, R_{\text{sigma}} = 0.0429$]	4106 [$R_{\text{int}} = 0.0922, R_{\text{sigma}} = 0.0540$]	4114 [$R_{\text{int}} = 0.1008, R_{\text{sigma}} = 0.0532$]
Data/restraints/parameters	4013/0/229	4099/0/229	4106/0/229	4114/0/229
Goodness-of-fit on F^2	1.017	1.034	1.014	1.030
Final R indexes [$ I \geq 2\sigma(I)$]	$R_1 = 0.0406, wR_2 = 0.0838$	$R_1 = 0.0332, wR_2 = 0.0693$	$R_1 = 0.0460, wR_2 = 0.1111$	$R_1 = 0.0342, wR_2 = 0.0767$
Final R indexes [all data]	$R_1 = 0.0961, wR_2 = 0.1041$	$R_1 = 0.0585, wR_2 = 0.0776$	$R_1 = 0.0983, wR_2 = 0.1365$	$R_1 = 0.0663, wR_2 = 0.0899$
Largest diff. peak/hole / $e \text{ \AA}^{-3}$	0.20/-0.31	0.32/-0.35	0.38/-0.57	0.39/-0.52

Table S2. The structural parameters of 5-7.

	5	6	7
Empirical formula	$C_{42}H_{40}N_4S_2ICu$	$C_{42}H_{40}N_4Se_2ICu$	$C_{22}H_{26}CuF_6N_6PS_2$
Formula weight	855.34	949.14	647.12
Temperature/K	273.15	273.15	273.15
Crystal system	monoclinic	monoclinic	triclinic
Space group	C2/c	C2/c	P-1
a/ \AA	28.154(6)	28.1758(15)	11.7935(7)
b/ \AA	10.252(2)	10.3689(4)	12.0809(7)
c/ \AA	14.169(3)	14.2314(6)	12.2924(7)
$\alpha/^\circ$	90	90	102.000(2)
$\beta/^\circ$	114.508(12)	115.236(3)	110.065(2)
$\gamma/^\circ$	90	90	111.341(2)
Volume/ \AA^3	3721.0(14)	3760.9(3)	1417.11(15)
Z	4	4	2
$\rho_{\text{calc}}/\text{cm}^3$	1.527	1.676	1.517
μ/mm^{-1}	1.565	3.373	1.037
F(000)	1736.0	1880.0	660.0
Crystal size/ mm^3	$0.28 \times 0.17 \times 0.17$	$0.28 \times 0.17 \times 0.17$	$0.08 \times 0.07 \times 0.06$
Radiation	MoK α ($\lambda = 0.71073$)	MoK α ($\lambda = 0.71073$)	MoK α ($\lambda = 0.71073$)
2 θ range for data collection/ $^{\circ}$	4.28 to 54.668	4.24 to 54.222	3.814 to 54.206
Index ranges	$-36 \leq h \leq 36, -13 \leq k \leq 13, -17 \leq l \leq 18$	$-36 \leq h \leq 36, -13 \leq k \leq 13, -18 \leq l \leq 18$	$-15 \leq h \leq 15, -15 \leq k \leq 15, -14 \leq l \leq 15$
Reflections collected	35507	42344	33022
Independent reflections	4179 [$R_{\text{int}} = 0.0665, R_{\text{sigma}} = 0.0380$]	4162 [$R_{\text{int}} = 0.0476, R_{\text{sigma}} = 0.0228$]	6254 [$R_{\text{int}} = 0.0605, R_{\text{sigma}} = 0.0438$]
Data/restraints/parameters	4179/0/229	4162/0/229	6254/0/347
Goodness-of-fit on F^2	1.038	1.026	1.018
Final R indexes [$ I \geq 2\sigma(I)$]	$R_1 = 0.0273, wR_2 = 0.0709$	$R_1 = 0.0241, wR_2 = 0.0518$	$R_1 = 0.0497, wR_2 = 0.1230$
Final R indexes [all data]	$R_1 = 0.0303, wR_2 = 0.0729$	$R_1 = 0.0339, wR_2 = 0.0551$	$R_1 = 0.0830, wR_2 = 0.1421$
Largest diff. peak/hole / $e \text{ \AA}^{-3}$	0.51/-0.73	0.47/-0.59	0.58/-0.51

Table 3. Selected bond lengths of **1-6**.

	1	2	3	4	5	6
			<i>Bond Lengths [Å]</i>			
C1-E1	1.708(2)	1.867(2)	1.719(3)	1.865(3)	1.7174(18)	1.867(2)
Cu1-E1	2.2603(7)	2.3742(4)	2.2583(14)	2.3661(4)	2.2544(6)	2.3654(3)
Cu1-X1	2.2555(11)	2.2426(12)	2.4036(14)	2.3883(7)	2.5793(7)	2.5641(5)

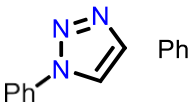
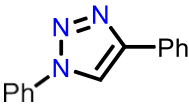
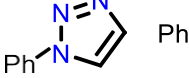
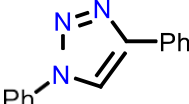
Table 4. Selected bond angles of **1-6**.

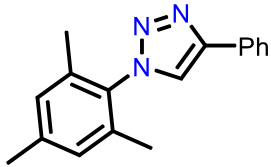
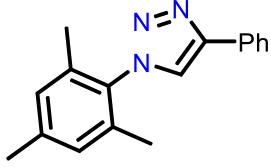
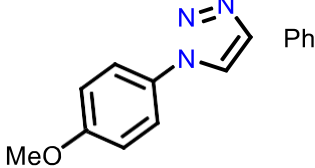
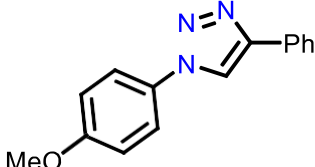
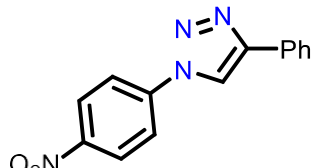
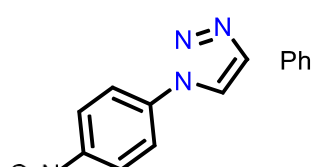
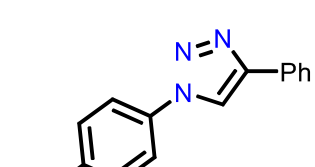
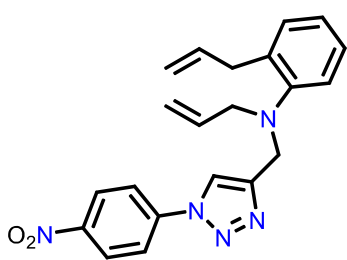
	1	2	3	4	5	6
			<i>Bond angles [°]</i>			
N1-C1-E1	127.0(2)	126.44(18)	126.7(3)	127.1(2)	126.79(14)	126.67(16)
C1-E1-Cu1	96.75(9)	93.43(7)	97.41(12)	93.85(8)	97.97(6)	94.34(6)
E1-Cu1-X1	120.76(2)	122.35(12)	118.59(3)	120.060(14)	116.610(16)	118.100(10)
E1-Cu1-E1'	118.48(4)	115.29(2)	122.83(6)	119.88(3)	126.78(3)	123.80(2)

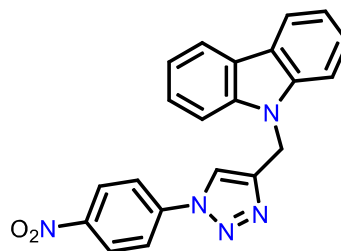
Table 5. Selected bond lengths (Å) and bond angles (°) of **7**.

<i>Bond length (Å)</i>		<i>Bond angle (°)</i>	
Cu1-S1	2.2476(10)	S1-Cu1-S2	128.82(4)
Cu1-S2	2.2721(9)	N3-Cu1-S1	95.92(8)
Cu1-N3	1.711(3)	N3-Cu1-S2	112.17(8)
Cu1-N4	2.124(3)	N3-Cu1-N4	116.25(11)
S1-C1	1.693(3)		

Table S6. Comparison of catalytic efficiency of **7** with known Cu(I) catalysts for the formation of triazole product.

Catalyst	Solvent	T/°C	t/h	Cu/mmol	Triazole product	Yield/%	ESI Ref.
CuI-USY	PhCH ₃	25 °C	15 h	10		59	1
[Cu(Bn2- imy)(IPr)]PF ₆	H ₂ O	60 °C	16 h	1		71	2
(MeCN) ₄ CuBF ₄	DCM	rt	24 h	5		46	3
Cat. 7	DCM:MeO H	25 °C	2 h	4		86	This work

[Cu(Bn2- imy)(IPr)]PF ₆	H ₂ O	60 °C	16 h	1		71	2
Cat.7	DCM:MeO H	25 °C	2 h	4		93	This work
[Cu]	H ₂ O	60 °C	16 h	1		83	1
Cat.7	DCM:MeO H	25 °C	2 h	4		91	This work
CuI	[bmim][BF 4]/ H ₂ O	25 °C	12 h	15		68	4
[Cu]	H ₂ O	60 °C	16 h	1		trace	1
Cat.7	DCM:MeO H	25 °C	2 h	4		82	This work
CuSO ₄ •5H ₂ O (20 mol%) sodium ascorbate (20 mol%)	Add t- butanol: water (1:1, v/v, 4 mL)	25 °C	8-10 h	20		87	



References

- 1 S. Chassaing, M. Kumarraja, A. Sani Souna Sido, P. Pale and J. Sommer, *Org. Lett.*, 2007, **9**, 883–886.
- 2 S. Guo, M. H. Lim and H. V. Huynh, *Organometallics*, 2013, **32**, 7225–7233.
- 3 K. Sugiyama, Y. Sakata, T. Niwa, S. Yoshida and T. Hosoya, *Chem. Commun.*, 2022, **58**, 6235–6238.
- 4 Y.-B. Zhao, Z.-Y. Yan and Y.-M. Liang, *Tetrahedron Letters*, 2006, **47**, 1545–1549.